Half-filled stripes in a hole-doped three-orbital spin-fermion model for cuprates

Mostafa Sherif Derbala Aly Hussein, Elbio Dagotto, and Adriana Moreo
Department of Physics and Astronomy, University of Tennessee, Knoxville, Tennessee 37966, USA
and Materials Science and Technology Division, Oak Ridge National Laboratory, Oak Ridge, Tennessee 37831, USA

(Received 17 December 2018; revised manuscript received 1 February 2019; published 6 March 2019)

Using Monte Carlo techniques, we study a three-orbital CuO_2 spin-fermion model for copper-based high-critical-temperature superconductors that captures the charge-transfer properties of these compounds. Our studies reveal the presence of spin order in the parent compound and, more importantly, stripe spin and charge order under hole doping. Due to the *p-d* orbital hybridization, the added holes are approximately equally distributed among the two *p* orbitals of the oxygen atoms and the *d* orbital of the copper atoms in the unit cell. In rectangular clusters of dimension 16×4 half-filled stripes are observed upon hole doping; namely, when $N_h = 2n$ holes are introduced in the system, then n vertical stripes of length 4 along the short periodic direction are formed. The original antiferromagnetic order observed in the parent compound develops a π shift across each stripe, and the magnetic structure factor has a peak at wave vector $\mathbf{k} = (\pi - \delta, \pi)$ with $\delta = 2\pi N_h/N = \pi N_h/2L$, where $L = 16$. The electronic charge is also modulated, and the charge structure factor is maximized at $\mathbf{k} = (2\delta, 0)$. As electrons are removed from the system, intracell orbital nematicity with $\langle n_{p_x}\rangle - \langle n_{p_y}\rangle \neq 0$ develops in the oxygen sector, as well as intercell magnetic nematicity with $\langle S^z_{\mathbf{i},d}(S^z_{\mathbf{i}+\mathbf{x},d} - S^z_{\mathbf{i}+\mathbf{y},d})\rangle \neq 0$ in the spin copper sector, in the standard notation. This occurs not only in rectangular but also in square 8×8 lattices. Our results suggest that the essence of the stripe spin and charge distribution experimentally observed in hole-doped cuprates is captured by unbiased Monte Carlo studies of a simple hole-doped charge-transfer insulator CuO_2 spin-fermion model.

DOI: 10.1103/PhysRevB.99.115108

I. INTRODUCTION

The parent compounds of the high-critical-temperature T_c superconducting cuprates are known to be charge-transfer insulators (CTIs) [1,2] with a band structure influenced by the hybridization of the $d_{x^2-y^2}$ orbital in the copper atoms and the $p_{\sigma=x,y}$ orbitals in the oxygen atoms. However, due to the technical difficulty of studying interacting many-body multiorbital Hubbard models, several of their properties, such as the incommensurate spin order and a tendency towards *d*-wave superconductivity upon doping, have been studied using simpler single-orbital systems, such as the one-orbital Hubbard and *t-J* models [2]. The use of single-orbital models relies on the Zhang-Rice singlet formalism that approximately maps a three-orbital Hubbard model into an effective *t-J* model [3] and also on the photoemission experimental observation of a single-band Fermi surface [4–7]. Despite the reasonably good agreement between numerical studies on one- and three-orbital models [8–10], several authors have claimed that the multiorbital CuO_2 character of the cuprates plays a crucial role in their physics that cannot be neglected [11,12]. While this issue is still being debated, it is clear that models that include the *p* oxygen orbitals, in addition to the *d* copper orbital, are more accurate and needed to study the problem of how the doped charges are distributed. Particularly in view of the charge-transfer character of the cuprates, doped electrons primarily are located into the Cu *d* orbitals, as in Mott insulators, while doped holes occupy, at least in part, the O *p* orbitals. In fact, from the Zaanen-Sawatzky-Allen paradigm [1], holes doped into a CTI should reside primarily, not only partially, in the *p* orbitals of the oxygens. This is the assumption made in the Zhang-Rice approach [3] as well. However, recent NMR experimental results appear to indicate that the hole distribution between *p* and *d* orbitals could be material dependent [13,14]. More work is clearly needed to clarify this matter.

In addition, there is strong theoretical and experimental interest in understanding the charge structure of the stripes observed in various hole-doped cuprates [15–20]. Early experimental results in single-layer $La_{2-x}Sr_xCuO_4$ (LSCO) at 1/8-hole doping clearly indicated the existence of nearly static *half-filled* stripes accompanied by magnetic order commensurate with the charge stripes [15–17]. On the other hand, in bilayer $YBa_2Cu_3O_7$ (YBCO), the magnetic and charge orders do not appear to coexist [18–20]. On the theory front, it was recently well established that the stripes stabilized in the ground state of the single-orbital Hubbard model are fully filled with holes [21], as opposed to half filled. This appears to be a general characteristic of various single-orbital models because it was already observed in a single-orbital spin-fermion model for the cuprates developed by some of us in the 1990s [22] and, more recently, in a frustrated *t-J* model as well [23]. Early indications of half-filled stripes observed with density matrix renormalization group (DMRG) [24] approaches in the one-orbital Hubbard models [25] are now attributed to a finite-width effect [21,26]. Nevertheless, we acknowledge that there are DMRG indications of half-filled stripes in the *t-J* model [27] and, more recently, in the Hubbard model if additional nearest-neighbor t' hoppings are added [28,29]. These extra hoppings physically originate in the O-O hopping intrinsic

in multiorbital systems. In our opinion, the differences in the conclusions using different models and techniques underscore the need to move beyond single-orbital models to better investigate the ground-state charge and magnetic properties of hole-doped cuprates and to guide the construction of one-orbital models that may capture the essence of the stripes.

However, studying multiorbital models is a very challenging task. Magnetic stripes were recently observed via quantum Monte Carlo (QMC) simulations of a three-orbital CuO_2 Hubbard model [30]. The simulations were performed using 8×8 and 16×4 clusters, as we do below. However, due to the sign problem, the studies were carried out at high temperature ($T \approx 1000$ K), considerably above the regime in which the charge structure of the stripes can be studied [30]. Also DMRG studies of the same model in 8×4 clusters, smaller than discussed in our publication and using external fields at the edges to stabilize the magnetic order, indicate the existence of half-filled stripes [31]. Because the above-mentioned QMC results are at high temperatures without charge order and the 8×4 DMRG calculations may be affected by size effects and need external fields for magnetic stabilization, simpler alternatives to try to capture the essence of the problem are worth investigating.

For this reason, in this paper we study a recently introduced simple three-orbital spin-fermion model [32] that captures the properties of the charge-transfer insulating parent compound of the cuprates and that can be studied upon doping in a wide range of temperatures and relatively large clusters. This seems ideal to explore at least qualitatively the charge and spin properties of doped cuprates. Our final goal is to find a simple model that captures the essence of the stripe formation, particularly with regard to its hole filling. A spin-fermion model can be considered as an *intermediate* approach between a crude mean-field approximation, where, typically, results are biased towards initial assumptions made, and a detailed unbiased, but technically very hard, QMC or DMRG approach.

Our publication is organized as follows: first, the model is described in Sec. II; then, the magnetic and charge structures observed upon hole doping are presented in Sec. III. Finally, Sec. IV is devoted to the conclusions. Overall, we believe that the simple spin-fermion CuO_2 model is able to capture the essence of the Cu oxide physics with regard to the hole-doped system and its magnetic and charge properties. Extensions of our model to lattices larger than those studied here are, in principle, doable using the traveling cluster approximation [33]. Moreover, the model and technique allow for the study of a wide range of temperatures, from very low to very high, the addition of quenched disorder, and even the study of real-time or real-frequency dynamical and dc transport properties. In these regards, we believe our effort opens a fertile area of research that will lead to qualitative progress in the study of Cu-based high-T_c superconductors and hole-doped charge-transfer insulators in general.

II. MODEL

In the present effort, the three-orbital spin-fermion model for the cuprates [32], which considers the $3d_{x^2-y^2}$ Cu and $2p_\sigma$ ($2p_x$ or $2p_y$) orbitals of the two oxygens in the CuO_2 unit cell, will be studied using primarily 8×8 and 16×4 clusters [34]. As described in our previous publication, the Hubbard repulsion at the Cu sites that splits the half-filled d band is replaced by an effective magnetic coupling between the spin of the itinerant electrons at the d orbital and phenomenological classical spins localized at the Cu sites. This is similar to the mean-field Monte Carlo approximation recently introduced [33], where the local mean-field parameters in the Hartree approximation (classical variables) are coupled to itinerant fully quantum fermions. Within this framework, an unbiased Monte Carlo simulation of the classical spins can be used to study the model. In this context, there are no sign problems, which means that the whole range of doping and temperatures can be explored. Since the resulting Hamiltonian is bilinear in the fermionic operators, clusters comparable to those employed for the full multiorbital Hubbard model were studied here, and using additional techniques, such as the traveling cluster approximation, substantially larger systems are potentially reachable in the future.

More specifically, the three-orbital spin-fermion (3SF) Hamiltonian is given by [32]

$$H_{3SF} = H_{TB} + H_{Sd} + H_{AF} + H_{Sp}, \tag{1}$$

with

$$\begin{aligned} H_{TB} &= -t_{pd} \sum_{\mathbf{i},\mu,\sigma} \alpha_{\mathbf{i},\mu} \left(p^\dagger_{\mathbf{i}+\frac{\hat{\mu}}{2},\mu,\sigma} d_{\mathbf{i},\sigma} + \text{H.c.} \right) \\ &\quad - t_{pp} \sum_{\mathbf{i},\langle\mu,\nu\rangle,\sigma} \alpha'_{\mathbf{i},\mu,\nu} \left[p^\dagger_{\mathbf{i}+\frac{\hat{\mu}}{2},\mu,\sigma} \left(p_{\mathbf{i}+\frac{\hat{\nu}}{2},\nu,\sigma} + p_{\mathbf{i}-\frac{\hat{\nu}}{2},\nu,\sigma} \right) + \text{H.c.} \right] \\ &\quad + \epsilon_d \sum_{\mathbf{i}} n^d_{\mathbf{i}} + \epsilon_p \sum_{\mathbf{i},\mu} n^p_{\mathbf{i}+\frac{\hat{\mu}}{2}} + \mu_e \sum_{\mathbf{i},\mu} \left(n^p_{\mathbf{i}+\frac{\hat{\mu}}{2}} + n^d_{\mathbf{i}} \right), \end{aligned} \tag{2}$$

where the operator $d^\dagger_{\mathbf{i},\sigma}$ creates an electron with spin σ at site $\mathbf{i}$ of the Cu square lattice, while $p^\dagger_{\mathbf{i}+\frac{\hat{\mu}}{2},\mu,\sigma}$ creates an electron with spin σ at orbital p_μ, where $\mu = x$ or y, for the oxygen located at $\mathbf{i} + \frac{\hat{\mu}}{2}$. The hopping amplitudes t_{pd} and t_{pp} correspond to the hybridizations between nearest-neighbor Cu-O and O-O, respectively, and $\langle \mu, \nu \rangle$ indicate O-O pairs connected by t_{pp}, as indicated in Fig. 1. $n^p_{\mathbf{i}+\frac{\hat{\mu}}{2},\sigma}$ ($n^d_{\mathbf{i},\sigma}$) is the number operator for p (d) electrons with spin σ, while ϵ_d and ϵ_p are the on-site energies at the Cu and O sites, respectively. $\Delta = \epsilon_d - \epsilon_p$ is the charge-transfer gap. The signs of the Cu-O and O-O hoppings due to the symmetries of the orbitals are included in the parameters $\alpha_{\mathbf{i},\mu}$ and $\alpha'_{\mathbf{i},\mu,\nu}$ and follow the convention shown in Fig. 1. The parameter values are set to $t_{pd} = 1.3$ eV and $t_{pp} = 0.65$ eV. The on-site energy is $\epsilon_p = -3.6$ eV [8], and thus, $\Delta = \epsilon_d - \epsilon_p$ is positive since we follow the convention $\epsilon_d = 0$. The electron chemical potential is μ_e. The remaining terms of H_{3SF} are

$$H_{Sd} = J_{Sd} \sum_{\mathbf{i}} \mathbf{S}_{\mathbf{i}} \cdot \mathbf{s}_{\mathbf{i}}, \tag{3}$$

where $\mathbf{S}_{\mathbf{i}}$ denotes the phenomenological localized spins at site $\mathbf{i}$ and $\mathbf{s}_{\mathbf{i}} = d^\dagger_{\mathbf{i},\alpha} \vec{\sigma}_{\alpha\beta} d_{\mathbf{i},\beta}$ is the spin of the mobile d electrons, with $\vec{\sigma}_{\alpha\beta}$ being the Pauli matrices. The other two terms

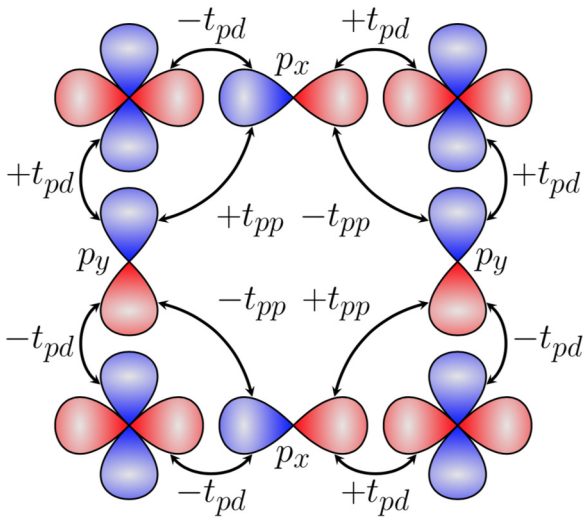

FIG. 1. Schematic drawing of the Cu $d_{x^2-y^2}$ orbitals at the copper sites of the square lattice, with the sign convention indicated by the colors (red for + and blue for −). The oxygen p_σ orbitals with their corresponding sign convention are also shown, located at the Cu-O-Cu bonds. The resulting sign convention for the t_{pd} and t_{pp} hoppings is also indicated.

are

$$H_{\rm AF} = J_{\rm AF} \sum_{\langle \mathbf{i},\mathbf{j}\rangle} \mathbf{S_i} \cdot \mathbf{S_j} \tag{4}$$

and

$$H_{\rm Sp} = J_{\rm Sp} \sum_{\mathbf{i},\hat{\mu}} \mathbf{S_i} \cdot \mathbf{s}_{\mathbf{i}+\frac{\hat{\mu}}{2}}, \tag{5}$$

where $\hat{\mu} = \pm\hat{x}$ or $\pm\hat{y}$ and $\mathbf{s}_{\mathbf{i}+\frac{\hat{\mu}}{2}} = p^{\dagger}_{\mathbf{i}+\frac{\hat{\mu}}{2},\mu,\alpha} \vec{\sigma}_{\alpha\beta} p_{\mathbf{i}+\frac{\hat{\mu}}{2},\mu,\beta}$.

As mentioned above, the localized spins are assumed to be classical [32], which allows $H_{\rm 3SF}$ to be studied with the same Monte Carlo procedure widely employed before for the pnictides [35] and double-exchange manganites [36]. The values of the couplings, specifically $J_{\rm AF} = 0.1$ eV, $J_{\rm Sp} = 1$ eV, and $J_{\rm Sd} = 3$ eV, were selected in our previous effort by comparing the orbital-resolved density of states with that of the three-orbital Hubbard model for cuprates obtained using the variational cluster approximation on a 12-site cluster [32]. The calculations shown below were performed using square 8×8 and rectangular 16×4 clusters [34] with periodic boundary conditions. These sizes are comparable to those accessible at present to study the three-band Hubbard model either via quantum Monte Carlo [37–39] or via DMRG [31], and the cluster sizes for the spin-fermion model can be increased substantially in the future. During the simulation the localized spins $\mathbf{S_i}$ evolve using a standard Monte Carlo procedure, while the resulting single-particle fermionic matrix is exactly diagonalized. The simulations are performed at inverse temperature $\beta = (k_B T)^{-1}$ ranging from 10 to 800 in eV^{-1}, equivalent to temperatures T from 1200 to 15 K [40]. In the electron representation, the undoped case corresponds to one hole at the Cu atoms and no holes at the O atoms, i.e., five electrons per CuO_2 unit cell (the maximum possible electronic number in three orbitals is six).

III. RESULTS

A. Charge and spin structures

The undoped system with five electrons per unit cell shows antiferromagnetically ordered localized spins and an almost uniform distribution of the electronic charge. For $\beta = 800$ eV^{-1} ($T \sim 15$ K) we found numerically that $\langle n_d \rangle = 1.164$ and $\langle n_{p_\sigma} \rangle = 1.918$, close but not identical to $\langle n_d \rangle = 1$ and $\langle n_{p_\sigma} \rangle = 2$, which would have been the values in the absence of p-d hybridization. These results are virtually independent of the cluster size used [34]. In Fig. 2(a), we display circles which are proportional to the local hole density given by $\langle n^h_{\mathbf{i},\alpha} \rangle = 2 - \langle n_{\mathbf{i},\alpha} \rangle$, with $\alpha = d$ or p_σ and $\mathbf{i}$ being the site index, using a 16×4 cluster at $T \sim 15$ K. The arrows denote the orientation of the localized spins in the x-z plane and clearly show the staggered antiferromagnetic order that develops [41]. This magnetic order also characterizes the mobile quantum spins at coppers, as shown by the peak at wave vector $\mathbf{k} = (\pi, \pi)$ that develops in the magnetic structure factor in Fig. 3(a) (triangles). The uniform charge distribution is indicated by the featureless charge structure factor $N(\mathbf{k})$ shown in Fig. 3(b) (triangles).

Consider now the case of doping corresponding to four holes. The charge is no longer uniformly distributed, as shown in Fig. 2(b), where the size of the circles is proportional to the difference between the density $n_{\mathbf{i},\alpha}$ and the corresponding electronic density in the undoped case [Fig. 2(a)] to better visualize the stripes. It is clear from Fig. 2(b) that two hole-rich stripes develop. To a good approximation, there are two holes per stripe, indicating that each stripe is half filled, as is the case in the real hole-doped cuprates according to neutron experiments [15–20]. Figure 3(b) (crosses) shows that a distinct feature appears in $N(\mathbf{k})$ at $\mathbf{k} = (\pi/4, 0) = (2\delta, 0)$, where δ indicates the displacement of the peak in the magnetic structure factor, which now is located at $\mathbf{k} = (\pi - \delta, \pi) = (7\pi/8, \pi)$, as shown in Fig. 3(a) (crosses). The incommensuration in the quantum spins indicates the presence of π shifts in the magnetic order across the stripes, which can also be observed visually in the planar projection of the classical spins in Fig. 2(b) [42].

The formation of additional half-filled stripes continues as more holes are added. For example, six (eight) holes form three (four) stripes, as shown in Figs. 2(c) and 2(d), respectively. The evolution of the magnetic and charge incommensurations δ with doping is also observed in Fig. 3, where the peaks in the structure factors continue to shift. Notice that for six holes (squares) the peak in $N(\mathbf{k})$ indicates that $2\delta = 3\pi/8$, but since $k = 3\pi/16$ is not allowed in the finite lattice used, the peak in $S(\mathbf{k})$, which should be at $(13\pi/16, \pi)$, is still located at $(7\pi/8, \pi)$ (squares). For eight holes (circles) $\delta = \pi/4$ from the peak in $N(\mathbf{k})$, and thus, $S(\mathbf{k})$ shows a peak at $(3\pi/4, \pi)$ which coexists with another peak at (π, π). Notice that eight holes corresponds to 1/8 doping in the 16×4 cluster, and the well-known $4a$ periodicity (with a being the lattice constant) is observed. The coexistence of the incommensurate peak with that at (π, π) for eight holes was found to be ubiquitous for this doping in our simulations. It appeared both when a random spin configuration was used as the starting point of the Monte Carlo simulation and when an ordered spin configuration with a maximum at $(3\pi/4, \pi)$

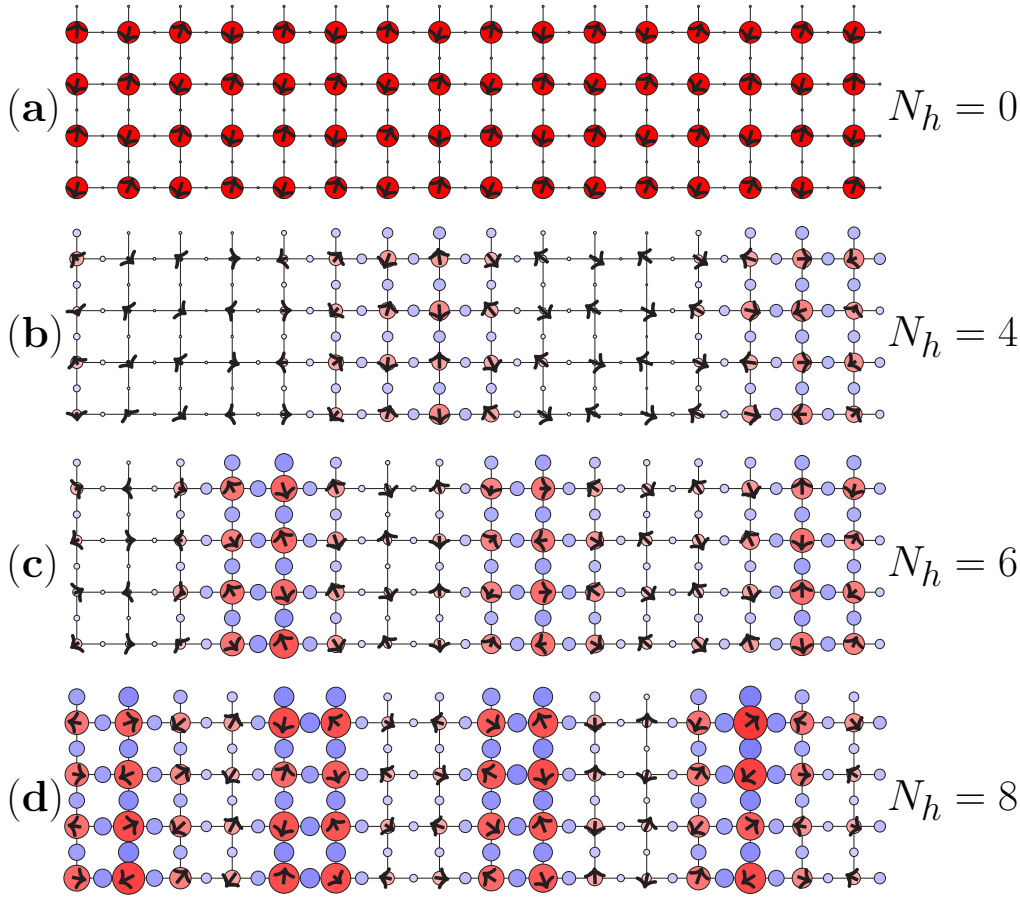

FIG. 2. Charge and spin configurations obtained with the spin-fermion model using $J_{AF} = 0.1\,\text{eV}$, $J_{Sp} = 1\,\text{eV}$, and $J_{Sd} = 3\,\text{eV}$ and employing 16×4 clusters at $\beta = 800\ \text{eV}^{-1}$ (i.e., $T \sim 15\,\text{K}$) for the following electronic densities: (a) the undoped case with five electrons (i.e., one hole) per unit cell, with the radius of the circles proportional to the hole charge, which is $n_d^h = 0.82$ in the Cu sites and $n_p^h = 0.09$ in the O sites (nearly uniform distribution) for the couplings used in our Hamiltonian, (b) results for four doped holes, (c) results for six doped holes, and (d) results for eight doped holes. In (b), (c), and (d) the radii of the circles are proportional to the difference between the electronic density in the doped system and that in the undoped case in (a) to better visualize the hole positions. The arrows in all panels are proportional to the classical spin projection in the x-z plane shown.

in the spin structure factor was used. In both cases, ordered and disordered starting spin configurations, the simulation converged to the same final state characterized by four charge stripes and the double-peaked magnetic structure which we found already present in the snapshots. Larger clusters, employing the traveling cluster approximation, will be needed in order to explore whether the peak at (π, π) arises from a finite-size effect.

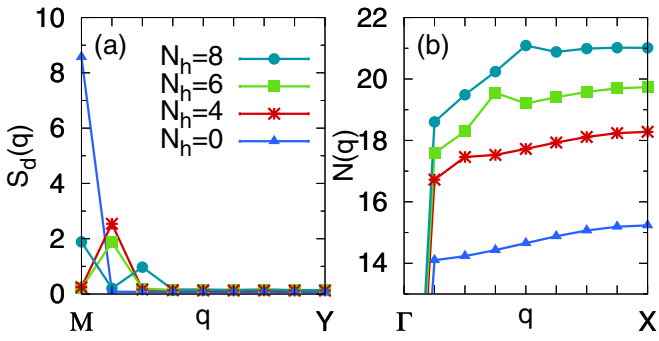

FIG. 3. (a) The magnetic structure factor $S_d(\mathbf{k})$ for the spin of the electrons in the Cu orbital along the M-Y direction in the spin-fermion model with $J_{AF} = 0.1\,\text{eV}$, $J_{Sp} = 1\,\text{eV}$, and $J_{Sd} = 3\,\text{eV}$, using a 16×4 cluster and $\beta = 800\ \text{eV}^{-1}$ ($T \sim 15\,\text{K}$) for the number of doped holes indicated in the legend. (b) The total charge structure factor $N(\mathbf{k})$ along the Γ-X direction for the same parameters as in (a).

B. Nematicity

Together with the stripes, an interesting feature that develops with doping is p-orbital nematicity. In Fig. 4(a) the orbital nematic order parameter, defined as $O_n = \langle n_{\mathbf{i},p_x} - n_{\mathbf{i},p_y} \rangle$, is shown vs the number of doped holes and for values of β ranging from 10 to 800 eV^{-1} (temperatures T ranging from $\sim$1200 to $\sim$15 K). As expected, there is no nematicity in the undoped system. However, it is clear that as hole doping increases and as the temperature decreases, then nematicity develops, with a larger hole occupation of the p orbitals in the direction parallel to the stripes. It can be argued that the nematicity is merely the result of the breaking of the rotational invariance due to the shape of the 16×4 clusters used here. However, a non-negligible nematic order parameter develops only at low temperatures and under hole doping. To further

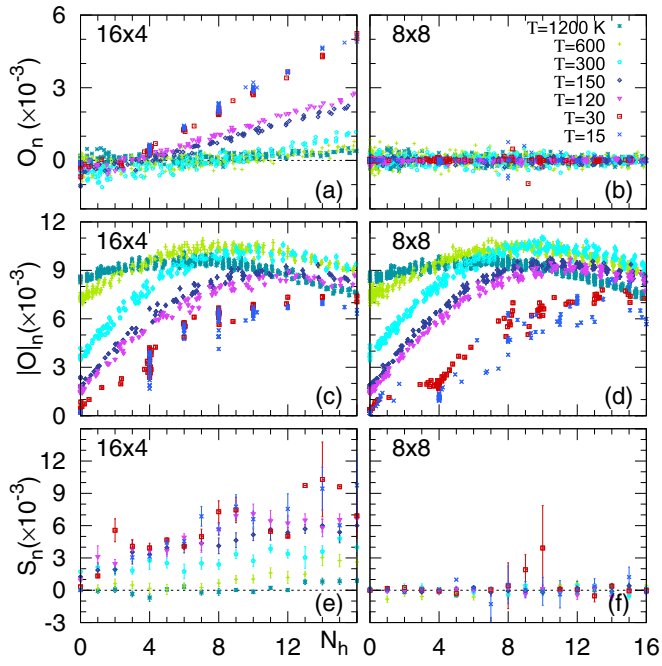

FIG. 4. Orbital nematic order parameter $O_n = \langle n_{\mathbf{i},p_x} - n_{\mathbf{i},p_y} \rangle$ varying the doped number of holes at the temperature T indicated in the legend, employing a spin-fermion model with $J_{\mathrm{AF}} = 0.1$ eV, $J_{\mathrm{Sp}} = 1$ eV, and $J_{\mathrm{Sd}} = 3$ eV. In (a) a 16×4 cluster is used. (b) is the same as (a), but employing an 8×8 cluster. In (c) the nematicity is given by $|O|_n = \langle |n_{\mathbf{i},p_x} - n_{\mathbf{i},p_y}| \rangle$ using a 16×4 cluster with the same parameters as in (a). (d) is the same as (c), but in an 8×8 cluster. (e) is the same as (a), but for the spin nematic order parameter $S_n = \langle S^z_{\mathbf{i},d}(S^z_{\mathbf{i}+\mathbf{x},d} - S^z_{\mathbf{i}+\mathbf{y},d}) \rangle$. (f) is the same as (e), but using an 8×8 cluster.

explore this issue we evaluated the nematicity in a *symmetric* 8×8 cluster. Here, no nematicity was observed in O_n [Fig. 4(b)], but this could be due to the coexistence of nematic regions with positive and negative values of O_n switching from one another during the Monte Carlo time evolution or simply a coherent quantum-mechanical superposition of both orientations.

To explore this possibility we studied the modified order parameter $|O|_n = \langle |n_{\mathbf{i},p_x} - n_{\mathbf{i},p_y}| \rangle$. This order parameter does *not* change sign if the orientation of the stripes switches from vertical to horizontal. While at high temperatures it is natural that thermal fluctuations locally establish a difference between the two directions from site to site, thus rendering $|O|_n$ nonzero even for zero holes, as the temperature is lowered, thermal fluctuations are reduced, and the order parameter $|O|_n$ becomes zero in the undoped limit because there are no stripes at temperatures sufficiently low. However, the results for the doped system are qualitatively different.

In Fig. 4(c) $|O|_n$ is plotted vs hole doping at various temperatures for the 16×4 cluster. As expected, its value decreases with temperature, and at $\beta = 400$ and 800 eV^{-1} (temperatures $T \sim 30$ and $\sim$15 K, respectively) the data for O_n in Fig. 4(a) are qualitatively reproduced (although with different slopes). The Monte Carlo results for $|O|_n$ in the 8×8 cluster are shown in Fig. 4(d). It is remarkable to observe that the curves are very *similar* to those for the 16×4 cluster in Fig. 4(c). In fact, in the undoped case it is clear that the order parameter $|O|_n$ for the square lattice converges to zero, as expected, at low temperatures where the thermal fluctuations are small, while it remains nonzero at finite doping even at the lowest temperatures investigated. This clearly supports the notion that the absence of stripes on the 8×8 cluster is due to a cancellation between both orientations, with each one dominating in different regions of the system. Local nematicity of the square lattice with periodic boundary conditions in both directions is present even at the lowest temperatures reached in our numerical simulations, but combining these results with the results shown in Fig. 4(b), we can deduce that in about 50% of the sites $n_{\mathbf{i},p_x} > n_{\mathbf{i},p_y}$ and vice versa. Namely, there is an asymmetry between the x and y directions. Again, it is also clear that there is no nematicity in the undoped system at low temperature, even using rectangular clusters that, in principle, break the lattice rotational invariance explicitly. However, the nematicity clearly increases with hole doping.

Scanning tunneling microscopy (STM) experiments have reported intracell nematicity in the p orbitals in underdoped $Bi_2Sr_2CaCu_2O_{8+\delta}$ (Bi-2212) [43] and in the overdoped regime of $(Bi,Pb)_2Sr_2CuO_{6+\delta}$ (Bi-2201) [44]. The nematicity found was attributed to inequivalence in the electronic structure at the two oxygen sites within each unit cell, but the experiments could not disentangle whether it was of charge or magnetic origin. Our results indicate that the nematicity arises from a charge difference among the intracell p_σ orbitals.

In addition, the previously mentioned STM experiments [43,44] did not observe nematicity associated with the d orbitals. However, the results of resonant x-ray scattering in the stripe phase of $(La,M)_2CuO_4$ (M=Sr, Ba, Eu, or Nd) [45] reported nematicity in the d orbitals. Our simulations indicate that the spin correlations among the spin of the electrons in the p orbitals are much smaller than those among the d electrons, and no magnetic nematicity in the p orbitals was observed. However, we studied the charge correlations along the x and y directions for the d orbital and its corresponding spin-nematic order parameter $S_n = \langle S^z_{\mathbf{i},d}(S^z_{\mathbf{i}+\mathbf{x},d} - S^z_{\mathbf{i}+\mathbf{y},d}) \rangle$. While no nematicity was observed in the charge correlations, we found that in the 16×4 cluster the nearest-neighbor antiferromagnetic correlations are stronger (weaker) in the direction parallel (perpendicular) to the stripes and the anisotropy increases when the temperature decreases, as shown in Fig. 4(e). The corresponding results in the 8×8 cluster [Fig. 4(f)] do not display nematicity, but we believe that, as in the orbital case [Fig. 4(b)], this is merely due to the equal presence of coexisting regions with both orientations of the nematicity. After all, if the charge patterns are an equal-weight mixture of vertical and horizontal stripes, the same has to occur for the spin textures.

We have also studied how the orbital nematicity and the magnetic and charge incommensurabilities develop vs temperature and doping. In the left column of Fig. 5 the orbital nematic order parameter O_n [Fig. 5(a)], the magnetic structure factor as its maximum value $\mathbf{k}_{\max} = (7\pi/8, \pi)$ [Fig. 5(d)], and the charge structure factor as its maximum value $\mathbf{k}_{\max} = (3\pi/4, 0)$ relative to its value at $\mathbf{k} = (\pi/8, 0)$ [Fig. 5(g)] are presented for the case of four doped holes in the 16×4 cluster. The three order parameters start developing at approximately the same temperature between 200 and 300 K. For

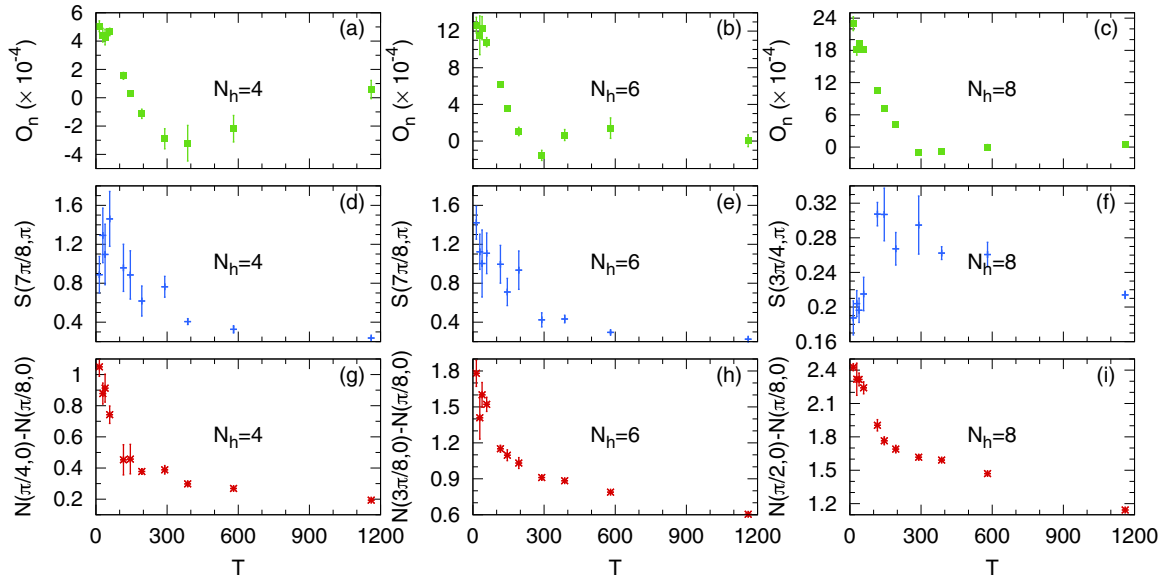

FIG. 5. Orbital nematic order parameter $O_n = \langle n_{\mathbf{i},p_x} - n_{\mathbf{i},p_y} \rangle$ vs temperature T for (a) four holes, $N_h = 4$, (b) six holes, $N_h = 6$, and (c) eight holes, $N_h = 8$. Also shown is the magnetic structure factor $S(\mathbf{k}_{\max})$ at the wave vector where it is maximized vs temperature for (d) $N_h = 4$ and $\mathbf{k}_{\max} = (7\pi/8, \pi)$, (e) $N_h = 6$ and $\mathbf{k}_{\max} = (7\pi/8, \pi)$, and (f) $N_h = 8$ and $\mathbf{k}_{\max} = (3\pi/4, \pi)$. Similarly, we present an analogous analysis for the charge. Shown is the maximum value of the charge structure factor $N(\mathbf{k}_{\max}) - N(\pi/8, 0)$ vs temperature for (g) $N_h = 4$ and $\mathbf{k}_{\max} = (\pi/4, 0)$, (h) $N_h = 6$ and $\mathbf{k}_{\max} = (3\pi/8, 0)$, and (i) $N_h = 8$ and $\mathbf{k}_{\max} = (\pi/2, 0)$. The results are for the spin-fermion model with $J_{\rm AF} = 0.1$ eV, $J_{\rm Sp} = 1$ eV, and $J_{\rm Sd} = 3$ eV using a 16×4 cluster.

six doped holes the corresponding results appear in Figs. 5(b), 5(e) and 5(h), and it can be observed that the three magnitudes start to increase at temperatures below $T \approx 300$ K. Finally, in Figs. 5(c), 5(f) and 5(i) the results for $N_h = 8$ are presented. Now the temperature below which the three order parameters start rising is lower, with $T \approx 200$ K.

These results seem to indicate that magnetic and charge incommensurabilities develop simultaneously with the nematicity. Thus, no purely isolated nematic phase is observed upon cooling. The presence of magnetic stripes at high temperature as reported in quantum Monte Carlo simulations of a three-band Hubbard model [30] is not detected by our approach either. We indeed used the approach in Ref. [30] to understand how the cluster geometry affects the formation of stripes. We measured the quantum spin-spin correlations for the d electrons $S^z(\ell, d) = \langle S^z_{\mathbf{i},d} S^z_{\mathbf{i}+\ell,d} \rangle$ in real space, and in Fig. 6(a) we display $(-1)^{|\ell_x+\ell_y|} S^z(\ell, d)$ in an 8×8 cluster at $\beta = 800\,\text{eV}^{-1}$ ($T \sim 15$ K) doped with eight holes. A structure consistent with coexisting vertical and horizontal half-filled stripes as in Ref. [30] is observed: near the origin of the coordinates (bottom left), the blue-toned points indicate a standard staggered spin pattern, while the red-toned points elsewhere indicate the presence of a π shift in the staggered pattern as it occurs in the presence of stripes. It is remarkable that a similar pattern is obtained in both the three-band Hubbard model and the three-band spin-fermion model using different numerical methods. However, we have identified these structures only at low temperatures, corresponding to the temperatures for which the stripes are well developed in the 16×4 clusters. In addition, in Fig. 6(b) it can be seen that the charge distribution is also consistent with the coexistence of one horizontal and one vertical half-filled stripe.

C. Total vs orbital doping

Finally, we want to address the issue of whether the properties of the cuprates should be discussed in terms of the total doping or instead focus on the local n_d and n_p dopings, as proposed in Refs. [13,14]. NMR measurements in different superconducting cuprates indicate that the change in the electronic density in the d and p orbitals as holes are added to the system is material dependent. In the undoped case, with one hole per unit cell, the hole would be expected to be located at the Cu atoms, so that the density of holes in the d orbitals $\langle n^h_d \rangle = 1$, while the density of holes in the p orbitals would be $\langle n^h_{p_x} \rangle = \langle n^h_{p_y} \rangle = 0$. However, experiments indicate that while the relationship $\langle n^h_d \rangle + \langle n^h_{p_x} \rangle + \langle n^h_{p_y} \rangle = 1$ is satisfied, the holes are distributed among the three orbitals in a hybridization-dependent way peculiar to each material, with $\langle n_d \rangle$ ranging from 0.82 for the case of La-214 (circles in Fig. 7) to about 0.68 for Y-123 (squares in Fig. 7) and finally to about 0.5 for Tl-2223 (green symbols in Fig. 7) [13,14].

The results for $\langle n^h_d \rangle$ versus $\langle n^h_{p_x} \rangle + \langle n^h_{p_y} \rangle$ measured in the spin-fermion model with the usual set of parameters are also plotted in Fig. 7 for various values of the inverse temperature β and for 16×4 and 8×8 clusters. Our results indicate that the orbital distribution of holes has a weak temperature dependence. We observed that the hole distribution between d and p electrons reproduces the experimental results for La-214 in the undoped case. Experimentally, it was also observed that the rate at which doped holes are distributed among the d and p orbitals is material dependent, and it is given by the slope of the curves shown in Fig. 7. The slope that we observed is larger than the one obtained experimentally for the Hg and Tl compounds, which, as shown in

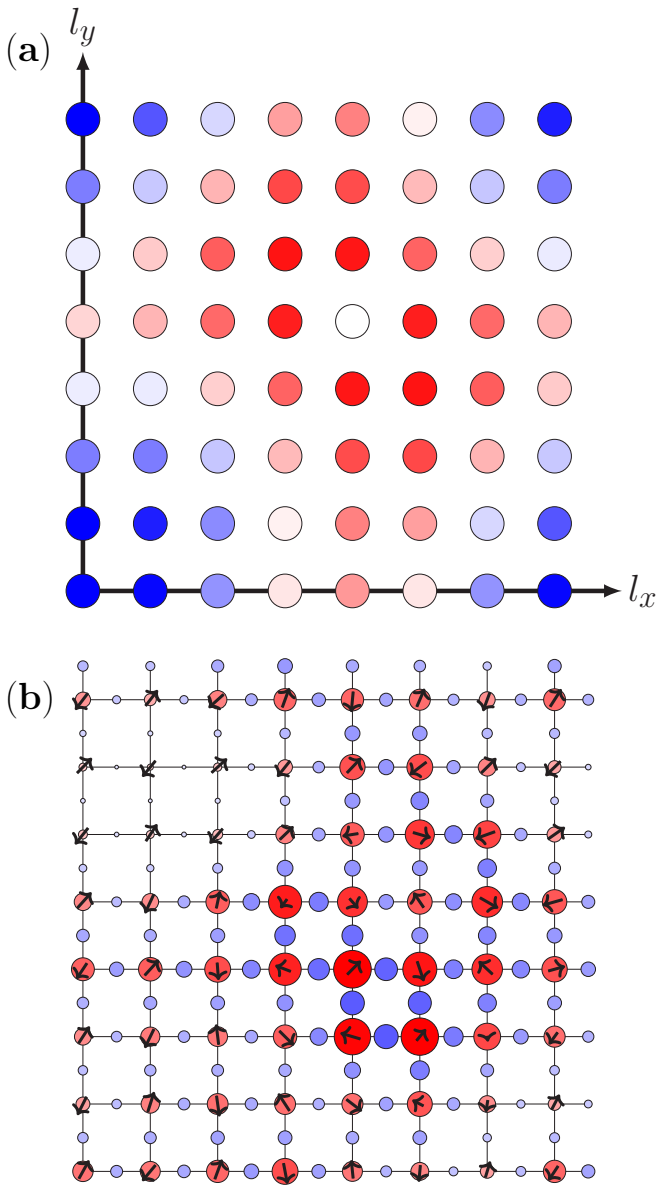

FIG. 6. (a) Real-space spin correlation functions $(-1)^{|\ell_x+\ell_y|}S^z(\ell, d)$ for the electrons in the d orbital using an 8×8 cluster with eight doped holes at $\beta = 800$ eV^{-1} ($T \sim 15$ K) and employing the spin-fermion model with $J_{\rm AF} = 0.1$ eV, $J_{\rm Sp} = 1$ eV, and $J_{\rm Sd} = 3$ eV. The blue-toned points near (0,0) (bottom left) indicate a standard spin antiferromagnetic pattern. The red-toned points indicate a spin correlation that has changed sign, namely, the presence of a π shift as it occurs in the presence of stripes. (b) Snapshot of the final configuration in a Monte Carlo run for the parameters in (a) showing the charge distribution and the classical spin projection in the x-z plane, as in Fig. 2.

Fig. 7, is slightly higher than the results for La-214 [13,14]. The parameters used in our calculations were obtained from comparisons with angle-resolved photoemission spectroscopy results obtained mostly in bismuth based cuprates [32] for which experimental results for $\langle n_d^h \rangle$ versus $\langle n_{p_x}^h \rangle + \langle n_{p_y}^h \rangle$ are not available. In this respect, the excellent agreement with LSCO results may be accidental. We believe that fine-tuning the parameters of the model, particularly in the tight-binding

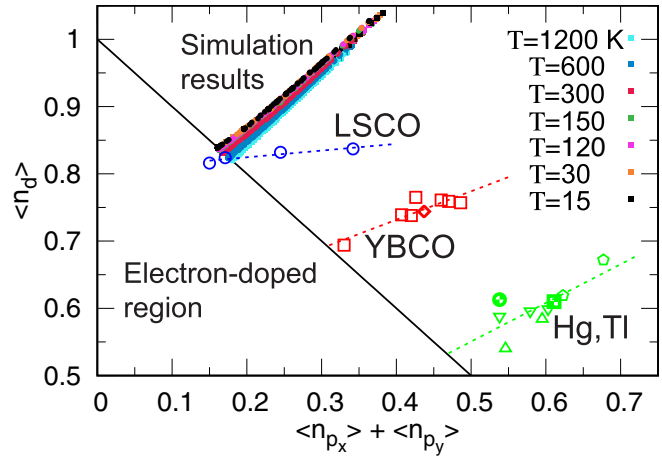

FIG. 7. Density of holes in the d orbital vs the total hole density in the p orbitals for the spin-fermion model with $J_{\rm AF} = 0.1$ eV, $J_{\rm Sp} = 1$ eV, and $J_{\rm Sd} = 3$ eV using 16×4 and 8×8 clusters for the temperatures indicated in the legend and for different hole densities, ranging from 0 holes (left) to 20 holes (right). The solid line indicates $\langle n_d \rangle + \langle n_{p_x} \rangle + \langle n_{p_y} \rangle = 1$, satisfied by the undoped system. Experimental results for hole-doped La-214 (LSCO; circles), Y-124 (diamonds) and Y-123 (squares; YBCO), and Hg- and Tl-based cuprates (green symbols; Hg-1201, Tl-2212, Tl-2223, and Tl-2201) were kindly provided by the authors of Ref. [13].

term, may improve quantitatively the agreement for all materials. However, it is important to notice that *qualitatively* the material-dependent distribution of the doped holes among the different orbitals in the unit cell is indeed captured by the spin-fermion model. This result indicates that some properties of the cuprates may be more dependent on the way in which the holes are distributed among the Cu and O orbitals than on the total density of doped holes.

IV. CONCLUSIONS

In this publication, we present the results of Monte Carlo studies of a phenomenological three-orbital CuO_2 spin-fermion model that captures the charge-transfer properties of the superconducting cuprates. The differences between a Mott and a charge-transfer insulator are relevant upon hole doping, the regime of main focus in our present study. One of the most peculiar properties of hole-doped cuprates is the formation of hole half-filled stripes (one hole every two sites along the stripe) [15–20,46–49], as opposed to hole fully filled stripes. This is a behavior that is not reproduced in the single-orbital Hubbard model [21,26], and it has been observed only in three-orbital Hubbard models using DMRG techniques in small clusters because of the numerical challenge represented by this formidable problem. Moreover, the quantum Monte Carlo studies of three-band Hubbard models can be performed only at temperatures above 1000 K due to sign problems, where charge stripes do not exist. Thus, it is important to find simpler alternatives that capture the qualitative essence of the problem without such computational complexity.

The present calculation obtains *half-filled charge stripes* with unbiased numerical calculations of a simple spin-fermion three-orbital charge-transfer system. In general, it is

difficult to study the stripes in square clusters because during the Monte Carlo time evolution both vertical and horizontal stripes develop, and the results represent *averages* in both directions. However, in rectangular 16×4 clusters the development of half-filled stripes, accompanied by magnetic π shifts across the stripes, is clear and properly captures the experimental results in the cuprates. In addition, we observed orbital nematicity due to an asymmetry in the charge distribution between the p_x and p_y orbitals in agreement with results from STM experiments [43,44]. Focusing on the copper d orbital, the nematicity observed with resonant x-ray scattering in the striped phase of $(La,M)_2CuO_4$ [45] was also found in our analysis.

Using 8×8 clusters and by focusing on the absolute value of the nematic order parameter, we unveiled tendencies towards half-filled stripes even in square clusters: the average over long runs appears featureless, but by using absolute values it can be shown that there is nematicity even in square clusters. One relatively minor problem in our study is that we found the issue of whether the stripes are centered at the d or the p orbitals difficult to address because the excess holes do not form sharp domains, as can be seen in Fig. 2; instead, they have a finite width.

These results also demonstrate the crucial role that the hybridization between the d copper orbitals and the p oxygen orbitals plays in the formation of half-filled stripes. In fact, in the limit in which the oxygen bands in the current model are pushed far away from the Fermi surface, the model becomes equivalent to the single-orbital spin-fermion model [22], which was studied before and has filled stripes. Our work also provides justification for the need to add a phenomenological plaquette diagonal hopping to the single-orbital Hubbard model in order to transition from the filled to the half-filled stripes recently reported [28,29]: the t' hopping captures the "bridge" effect to allow diagonal electronic movement among the d orbitals provided by the p orbitals at the oxygens.

The correct magnetic properties are also captured by the spin-fermion model that displays clear tendencies towards long-range antiferromagnetic order in the undoped case, and it also starts to develop incipient indications of incommensurability along $(\pi - \delta, \pi)$ and $(\pi, \pi - \delta)$ in the doped case. The coexistence of charge and magnetic orders is material dependent in the cuprates, and in the present model, it is possible that these properties could be captured by modifications of the parameters. In addition, these particular features that develop upon hole doping likely originate in stripes, although they could also result from intertwined orders, and they appear to require rectangular clusters for their proper stabilization. Future work will address even larger lattices (employing techniques developed for spin-fermion-like models in contexts such as manganites), a detailed temperature dependence, and the influence of quenched disorder on the appearance of stripes in CuO_2 spin-fermion models.

ACKNOWLEDGMENTS

All members of this collaboration were supported by the U.S. Department of Energy (DOE), Office of Science, Basic Energy Sciences (BES), Materials Sciences and Engineering Division.

[1] J. G. Zaanen, G. A. Sawatzky, and J. W. Allen, Phys. Rev. Lett. **55**, 418 (1985).
[2] E. Dagotto, Rev. Mod. Phys. **66**, 763 (1994), and references therein.
[3] F. C. Zhang and T. M. Rice, Phys. Rev. B **37**, 3759 (1988).
[4] Z.-X. Shen, J. W. Allen, J. J. Yeh, J.-S. Kang, W. Ellis, W. Spicer, I. Lindau, M. B. Maple, Y. D. Dalichaouch, M. S. Torikachvili, J. Z. Sun, and T. H. Geballe, Phys. Rev. B **36**, 8414 (1987).
[5] J. W. Allen, C. G. Olson, M. B. Maple, J.-S. Kang, L. Z. Liu, J.-H. Park, R. O. Anderson, W. P. Ellis, J. T. Markert, Y. Dalichaouch, and R. Liu, Phys. Rev. Lett **64**, 595 (1990).
[6] B. O. Wells, Z.-X. Shen, A. Matsuura, D. M. King, M. A. Kastner, M. Greven, and R. J. Birgeneau, Phys. Rev. Lett **74**, 964 (1995).
[7] A. Damascelli, Z. Hussain, and Z.-X. Shen, Rev. Mod. Phys. **75**, 473 (2003).
[8] M. S. Hybertsen, M. Schlüter, and N. E. Christensen, Phys. Rev. B **39**, 9028 (1989).
[9] S. B. Bacci, E. R. Gagliano, R. M. Martin, and J. F. Annett, Phys. Rev. B **44**, 7504 (1991).
[10] E. Arrigoni, M. Aichhorn, M. Daghofer, and W. Hanke, New J. Phys. **11**, 055066 (2009).
[11] V. J. Emery, Phys. Rev. Lett. **58**, 2794 (1987).
[12] B. Lau, M. Berciu, and G. A. Sawatzky, Phys. Rev. Lett. **106**, 036401 (2011).
[13] M. Jurkutat, D. Rybicki, O. P. Sushkov, G. V. M. Williams, A. Erb, and J. Haase, Phys. Rev. B **90**, 140504(R) (2014).
[14] D. Rybicki, M. Jurkutat, S. Reichardt, C. Kapusta, and J. Haase, Nat. Commun. **7**, 11413 (2016).
[15] J. M. Tranquada, B. Sternlieb, J. Axe, Y. Nakamura, and S. Uchida, Nature (London) **375**, 561 (1995).
[16] R. J. Birgeneau, C. Stock, J. M. Tranquada, and K. Yamada, J. Phys. Soc. Jpn. **75**, 111003 (2006).
[17] J. M. Tranquada, Phys. B (Amsterdam, Neth.) **407**, 1771 (2012).
[18] S. Blanco-Canosa, A. Frano, T. Loew, Y. Lu, J. Porras, G. Ghiringhelli, M. Minola, C. Mazzoli, L. Braicovich, E. Schierle, E. Weschke, M. Le Tacon, and B. Keimer, Phys. Rev. Lett. **110**, 187001 (2013).
[19] M. Hücker, N. B. Christensen, A. T. Holmes, E. Blackburn, E. M. Forgan, R. Liang, D. A. Bonn, W. N. Hardy, O. Gutowski, M. V. Zimmermann, S. M. Hayden, and J. Chang, Phys. Rev. B **90**, 054514 (2014).
[20] S. Blanco-Canosa, A. Frano, E. Schierle, J. Porras, T. Loew, M. Minola, M. Bluschke, E. Weschke, B. Keimer, and M. Le Tacon, Phys. Rev. B **90**, 054513 (2014).
[21] B.-X. Zheng, C.-M. Chung, P. Corboz, G. Ehlers, M.-P. Qin, R. M. Noack, H. Shi, S. R. White, S. Zhang, and G. K.-L. Chan, Science **358**, 1155 (2017).
[22] C. Buhler, S. Yunoki, and A. Moreo, Phys. Rev. Lett. **84**, 2690 (2000).

[23] J. F. Dodaro, H.-C. Jiang, and S. A. Kivelson, Phys. Rev. B **95**, 155116 (2017).
[24] S. R. White, Phys. Rev. Lett. **69**, 2863 (1992); Phys. Rev. B **48**, 10345 (1993).
[25] S. R. White and D. J. Scalapino, Phys. Rev. Lett. **91**, 136403 (2003).
[26] G. Ehlers, S. R. White, and R. M. Noack, Phys. Rev. B **95**, 125125 (2017).
[27] S. R. White and D. J. Scalapino, Phys. Rev. Lett. **80**, 1272 (1998).
[28] E. W. Huang, C. B. Mendl, H. C. Jiang, B. Moritz, and T. P. Devereaux, npj Quantum Mater. **3**, 22 (2018).
[29] H.-C. Jiang and T. P. Devereaux, arXiv:1806.01465.
[30] E. W. Huang, C. B. Mendl, S. Liu, S. Johnston, H.-C. Jiang, B. Moritz, and T. P. Devereaux, Science **358**, 1161 (2017).
[31] S. R. White and D. J. Scalapino, Phys. Rev. B **92**, 205112 (2015).
[32] M. S. D. A. Hussein, M. Daghofer, E. Dagotto, and A. Moreo, Phys. Rev. B **98**, 035124 (2018).
[33] A. Mukherjee, N. D. Patel, S. Dong, S. Johnston, A. Moreo, and E. Dagotto, Phys. Rev. B **90**, 205133 (2014); A. Mukherjee, N. D. Patel, C. Bishop, and E. Dagotto, Phys. Rev. E **91**, 063303 (2015).
[34] Some runs in 12×6 and 12×8 clusters were also performed, corroborating the results obtained in the smaller clusters.
[35] S. Liang, A. Moreo, and E. Dagotto, Phys. Rev. Lett. **111**, 047004 (2013); See also S. Liang, G. Alvarez, C. Sen, A. Moreo, and E. Dagotto, *ibid.* **109**, 047001 (2012).
[36] E. Dagotto, S. Yunoki, A. L. Malvezzi, A. Moreo, J. Hu, S. Capponi, D. Poilblanc, and N. Furukawa, Phys. Rev. B **58**, 6414 (1998).
[37] G. Dopf, A. Muramatsu, and W. Hanke, Phys. Rev. B **41**, 9264 (1990).
[38] Z. B. Huang, H. Q. Lin, and J. E. Gubernatis, Phys. Rev. B **63**, 115112 (2001).
[39] Y. F. Kung, C.-C. Chen, Y. Wang, E. W. Huang, E. A. Nowadnick, B. Moritz, R. T. Scalettar, S. Johnston, and T. P. Devereaux, Phys. Rev. B **93**, 155166 (2016).
[40] The temperature T (in degrees Kelvin) is obtained using $T = 11\,605/\beta$.
[41] The spins of the electrons in the d orbital are oriented antiparallel to the classical spins.
[42] The π shift in the classical spins manifests itself as a slow rotation.
[43] M. J. Lawler, K. Fujita, J. Lee, A. R. Schmidt, Y. Kohsaka, C. K. Kim, H. Eisaki, S. Uchida, J. C. Davis, J. P. Sethna, and E-A. Kim, Nature (London) **466**, 347 (2010).
[44] Y. Zheng, Y. Fei, K. Bu, W. Zhang, Y. Ding, X. Zhou, J. E. Hoffman, and Y. Yin, Sci. Rep. **7**, 8059 (2017).
[45] A. J. Achkar, M. Zwiebler, C. McMahon, F. He, R. Sutarto, I. Djianto, Z. Hao, M. J. P. Gingras, M. Hücker, G. D. Gu, A. Revcolevschi, H. Zhang, Y.-J. Kim, J. Geck, and D. G. Hawthorn, Science **351**, 576 (2016).
[46] S. W. Cheong, G. Aeppli, T. E. Mason, H. Mook, S. M. Hayden, P. C. Canfield, Z. Fisk, K. N. Clausen, and J. L. Martinez, Phys. Rev. Lett **67**, 1791 (1991).
[47] J. M. Tranquada, J. D. Axe, N. Ichikawa, A. R. Moodenbaugh, Y. Nakamura, and S. Uchida, Phys. Rev. Lett. **78**, 338 (1997).
[48] P. Dai, H. A. Mook, and F. Dogan, Phys. Rev. Lett **80**, 1738 (1998).
[49] H. A. Mook, P. Dai, S. M. Hayden, G. Aeppli, T. G. Perring, and F. Dogan, Nature (London) **395**, 580 (1998).